

April 2000

ULG-PNT-00-1-IR

Helicity in diffractive vector-meson production.

I. Royen¹

Inst. de Physique, U. de Liège, Bât. B-5, Sart Tilman, B4000 Liège, Belgium

Abstract

We study the helicity amplitudes describing the quasielastic production of vector mesons in deep inelastic scattering within the context of the model which we previously introduced to describe the ratio of longitudinal to transverse cross sections. We calculate here a full set of spin flip (and non-flip) amplitudes and naturally find a significant violation of s-channel helicity conservation. We present predictions for the 15 spin-density matrix elements which completely define the angular distributions and the helicity properties of the produced meson.

¹royen@nuclth02.phys.ulg.ac.be

1 Introduction

Elastic vector meson production in photon-proton scattering $\gamma^*p \rightarrow Vp$ is an important process under intensive experimental and theoretical study. It should provide us with information on the quark and gluon structure of hadrons as well as information on the exchange forces between the particles in this process.

From many papers (see references in [1]), it turns out that perturbative QCD models where pomeron is represented by two-gluon exchange are able to reproduce the main features of the HERA data. In a previous paper [2], with J.R. Cudell, we implemented Fermi momentum in elastic vector-meson production and proposed a new approach which allows the quarks to be off-shell, and which naturally reproduces the data. The Q^2 and m_V dependence of the dominant transitions $\gamma_L^* \rightarrow V_L$ and $\gamma_T^* \rightarrow V_T$ are in good agreement with the data and the model naturally reproduces the ratio σ_L/σ_T (L and T stand for the longitudinal and transverse polarisations). The plateau observed experimentally comes from the interplay between contributions from on-shell and off-shell quarks, which have different asymptotic behaviours.

The aim of this paper is to explore the polarisation effects in quasielastic electro-production of vector mesons within the framework of the above model. We know that the cross section for the exclusive production of vector mesons from virtual photon has contributions from both transverse and longitudinal photons. What about the spin of the produced meson ? Experimentally, information about the polarisation state of the produced meson is extracted from the angular distributions of the meson decay products ($\pi^+\pi^-$ for the ρ meson). Previous studies at HERA [3, 4] were consistent with s-channel helicity conservation (SCHC), i.e. the produced meson retains the helicity of the incoming virtual photon. Sufficient data are now available to test the validity of SCHC at HERA by measuring the full set of matrix elements which completely determine the angular distributions of the decay. As a consequence, H1 [5] and ZEUS [6] have found a small but significant violation of SCHC in ρ meson production.

Following the formalism introduced by Schillings [7], the 15 spin density matrix elements, $r_{ij}^{\alpha\beta}$, which completely define the angular distributions $W(\rho \rightarrow \pi^+\pi^-)$, are related to various combinations of the helicity amplitudes $A_{\lambda_V\lambda_N,\lambda_\gamma\lambda_{N'}}$, where λ_V and λ_γ are, respectively, the helicities of the vector meson and of the photon, and λ_N and $\lambda_{N'}$ those of the incoming and outgoing proton (see appendix).

To get a feeling for these amplitudes we can consider some special cases, as well as general constraints.

- Under parity conservation in the t -channel, the helicity amplitudes yield the following symmetry relation:

$$A_{-\lambda_V \lambda_{p'}, -\lambda_\gamma \lambda_p} = (-1)^{\lambda_V - \lambda_\gamma} A_{\lambda_V \lambda_{p'}, \lambda_\gamma \lambda_p}. \quad (1)$$

There are then five independent helicity amplitudes: the two helicity conserving amplitudes, two single spin-flip amplitudes and one helicity double-flip amplitude²:

$$A_{V_L \gamma_L^*} = A_{00}, \quad (2)$$

$$A_{V_T \gamma_T^*} = A_{11} = A_{-1-1}, \quad (3)$$

$$A_{V_L \gamma_T^*} = A_{01} \text{ with } A_{0-1} = -A_{01}, \quad (4)$$

$$A_{V_T \gamma_L^*} = A_{10} \text{ with } A_{-10} = -A_{10}, \quad (5)$$

$$\text{and } A_{-11} = A_{1-1} \quad (6)$$

- Under the assumption of s -channel helicity conservation (SCHC), the helicity of the virtual photon is retained by the vector meson V :

$$A_{\lambda_V \lambda_{p'}, \lambda_\gamma \lambda_p} = A_{\lambda_V \lambda_{p'}, \lambda_\gamma \lambda_p} \delta_{\lambda_V \lambda_\gamma} \delta_{\lambda_{p'} \lambda_p}. \quad (7)$$

There are only two independent helicity amplitudes, single and double helicity flip amplitudes are then zero:

$$A_{\lambda_V \lambda_\gamma} = 0, \quad \lambda_V \neq \lambda_\gamma \quad (8)$$

The assessment of the validity of this last assumption is the object of this letter.

Theoretical studies of helicity amplitudes for diffractive production of vector meson at large Q^2 have first been performed by Ivanov and Kirschner [8], and later by Nikolaev et al [9] using perturbative QCD, and extending the QCD factorisation theorem. Although there is no longer any doubt about the dominance of transitions $\gamma_L^* \rightarrow V_L$ and $\gamma_T^* \rightarrow V_T$, they reported a substantial s -channel helicity non conservation. They assumed that all helicity amplitudes (except the double-flip) are proportional to the gluon structure function of the proton and they agree that the largest amplitude violating SCHC is A_{10} , where a transverse photon produce a longitudinal vector meson.

² We shall discuss reactions with unpolarised protons, therefore the proton can be formally considered as a spinless target and we shall indicate only the polarisation states of the virtual photon and the produced meson. L and T stand then for the longitudinal and transverse polarisations.

This study differs from the previous ones as now all helicity properties are coming from the transition $\gamma^* \rightarrow V$ only. Hence in this paper, we concentrate only on the upper diagram (Fig. 1), following our previous model [2] to calculate all helicity amplitudes, we extend our results to lower Q^2 and we derive the 15 matrix elements to be compared with the data. We first present the main steps of the model described in [2] and calculate the helicity amplitudes. Their properties are given in section 3. In section 4, we calculate the matrix elements to compare with the data. We summarise our conclusions in section 5.

2 Kinematics and calculation of the different helicity amplitudes.

One usually assumes that the exclusive process at high energy proceeds from the emission of a pair of gluons from the proton, which interact with a $q\bar{q}$ pair emerging from the photon, and which transfer momentum so that this pair can be turned into a vector meson, as shown in Fig. 1. The following kinematic variables are used to describe the problem $\gamma^* p \rightarrow V p$ [2]. The photon has 4-momentum q and polarisation $\epsilon(\lambda_\gamma)$, with $q \cdot q = -Q^2$. We define

$$\epsilon(\lambda_\gamma = \pm 1) = \mp(1/\sqrt{2})(0, 1, \pm i, 0) \quad (9)$$

which correspond to circularly polarised radiation for transverse photons and

$$\epsilon(\lambda_\gamma = 0) = (1/\sqrt{Q^2})(q^3, 0, 0, q^0) \quad (10)$$

for longitudinal photons. The hard process generating the meson, and the $q\bar{q} \rightarrow V$ amplitude are treated together through the introduction of a meson vertex function. The gluons will couple to the quarks emerging from this vertex. The vector meson has momentum $V = q + \Delta$ and polarisation $e(\lambda_V)$ defined in the same way as $\epsilon(\lambda_\gamma)$. With $t = \Delta^2$, $V^2 = m_V^2$, hence $\Delta \cdot q = (m_V^2 - t + Q^2)/2$. The quarks composing the meson are written as $v + l$ and $-v + l$ with $v = V/2$.

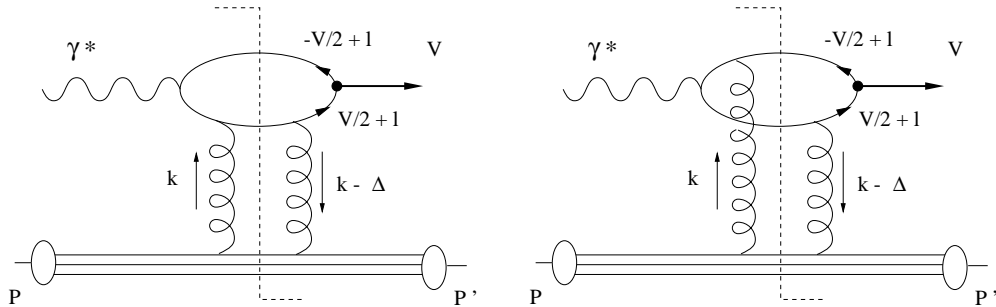


Figure 1: The two diagrams accounting for the transition $\gamma p \rightarrow V p$. The dashed line represents the cut which puts the intermediate state on-shell.

We assume the vertex function to be described by:

$$\Gamma_\mu = \Phi(l)\gamma_\mu \quad (11)$$

$$\text{with } \Phi(l) = N e^{\frac{-b_f L^2}{2p_F^2}} \quad (12)$$

where \mathbf{L}^2 is the quark 3-momentum in the meson rest frame, and where p_F is a Fermi momentum scale equal to 0.3 GeV in the ρ and ϕ cases. As we do

not want to look in detail at the scattered proton, we only consider its three valence quarks of momentum p , we assume that we can neglect its mass and we put it on-shell $p.p = 0$. Moreover, we introduce the following form factor $\mathcal{F}(k, \Delta) = 3(\mathcal{E}_1(t) - \mathcal{E}_2(k, k - \Delta))$ where:

$$\mathcal{E}_1(t = \Delta^2) \simeq \frac{(3.53 - 2.79t)}{(3.53 - t)(1 - t/0.71)^2} \quad (13)$$

is the quark-level form factor when both gluons hit the same quark line, and

$$\mathcal{E}_2(k, k - \Delta) = \mathcal{E}_1(k^2 + (k - \Delta)^2 - k.(k - \Delta)) \quad (14)$$

if the gluons hit different quark lines. These form factors, which take the dipolar character of the proton into account, are necessary to obtain IR finiteness.

This model allows us to calculate all the helicity amplitudes with and without spin flip between the photon and the vector meson. We shall be working in the high- w^2 limit, and we write $p.q = (p+q)^2/2 \approx w^2/2$. As we expect the amplitude to be w -independent, we shall be calculating the discontinuity of the amplitude using Cutkovsky's rules and putting the intermediate quark propagators on-shell. The transition amplitude is given by the convolution between the upper diagrams and the lower diagrams (Fig. 1):

$$\begin{aligned} A_{\lambda_V \lambda_\gamma} &= \frac{2}{3} (4\pi\alpha_S)^2 g^{elm} e_Q w^2 \\ &\times \int \frac{d^4 l}{(2\pi)^4} \frac{d^4 k}{(2\pi)^4} \mathcal{F}(k, \Delta) \frac{1}{\sqrt{3}} \Phi(l) \\ &\times \frac{4(p_\alpha p_\beta) T_{\lambda_V \lambda_\gamma}^{\alpha\beta}}{k^2(k - \Delta)^2}. \end{aligned} \quad (15)$$

where $4(p_\alpha p_\beta)$ is the leading contribution of the lower quark lines and $T^{\alpha\beta}$ the sum of the two cut diagrams:

$$\begin{aligned} T^{\alpha\beta} &= \left[\frac{T_1^{\alpha\beta}(\epsilon, e)}{(q - v + l).(q - v + l) - m_q^2} + \frac{T_2^{\alpha\beta}(\epsilon, e)}{(-v + l + k).(-v + l + k) - m_q^2} \right] \\ &\times \frac{((2\pi)^2 \delta((-v + l)^2 - m_q^2) \delta((v + l + k - \Delta)^2 - m_q^2))}{(v + l)^2 - m_q^2}. \end{aligned} \quad (16)$$

Following [2], the traces of the upper bubbles of the graphs are described by:

$$\begin{aligned} T_1^{\alpha\beta} &= Tr\{\gamma.e[\gamma.(v + l) - m_q]\gamma_\beta[\gamma.(q - v + l + k) + m_q]\gamma^\alpha \\ &\times [\gamma.(q - v + l) + m_q]\gamma.\epsilon[\gamma.(-v + l) + m_q]\} \end{aligned} \quad (17)$$

$$\begin{aligned} T_2^{\alpha\beta} &= Tr\{\gamma.e[\gamma.(v - l) - m_q]\gamma_\alpha[\gamma.(v - l - k) + m_q]\gamma^\epsilon \\ &\times [\gamma.(v - q - k - l) + m_q]\gamma.\beta[\gamma.(-v - l) + m_q]\} \end{aligned} \quad (18)$$

Using equation (15), we calculate:

- the longitudinal vector meson production amplitude by a longitudinal photon: $T_{\lambda_V \lambda_\gamma} = T_{00}$,
- the transverse-vector-meson-production amplitude by a transverse photon:
 - with single-spin flip: $T_{\lambda_V \lambda_\gamma} = T_{11}, T_{-1-1}$,
 - with double-spin flip: T_{1-1}, T_{-11} ,
- single-spin-flip helicity amplitudes where:
 - a transverse photon produces a longitudinal meson:
 $T_{\lambda_V \lambda_\gamma} = T_{01}, T_{0-1}$,
 - a longitudinal photon produces a transverse meson:
 $T_{\lambda_V \lambda_\gamma} = T_{10}, T_{-10}$.

2.1 SCHC amplitudes.

The results obtained with this model confirm the dominance of the longitudinal amplitude T_{00} at high Q^2 , in agreement with [10, 11, 12]. In the high-energy w limit, defining $l = \frac{\alpha}{2w^2}p + \frac{\beta}{2}q + \frac{1_t}{2}$ and $k = \frac{\zeta}{2w^2}p + \frac{\xi}{2w^2}q + \frac{1_t}{2}$, the longitudinal-vector-meson-production amplitude by a longitudinal photon T_{00} is the following:

$$T_{00} = \frac{-4(\mu_q^2 + (1 - \beta^2)m_V^2 - \mathbf{l}_t^2)(1 + \beta)^2(1 - \beta)Q\epsilon_L \cdot e_L}{[(1 - \beta)^2 t - \mu_q^2 + \mathbf{l}_t^2 - (1 - \beta^2)Q^2 - 2(1 - \beta)\mathbf{l}_t \cdot \Delta_t]m_V} \times \frac{2(1 - \beta)\mathbf{k}_t \cdot \Delta_t - 2\mathbf{k}_t \cdot \mathbf{l}_t + \mathbf{k}_t^2}{D(Q^2, t, k_t, l_t)} \quad (19)$$

where

$$D(Q^2, t, k_t, l_t) \equiv [(1 - \beta^2)Q^2 - (1 - \beta)^2 t + \mu_q^2 - \mathbf{l}_t^2 + \mathbf{k}_t^2 + 2(1 - \beta)\mathbf{k}_t \cdot \Delta_t - 2\mathbf{k}_t \cdot \mathbf{l}_t + 2(1 - \beta)\mathbf{l}_t \cdot \Delta_t]. \quad (20)$$

and $\mu_q = 2m_q$ the mass of the quarks in the upper loop of the diagram.

The transverse amplitude T_{11} ($\lambda_V = \lambda_\gamma = +1$), is more complicated. To give an analytical expression, we shall concentrate on the case $t = 0$ [2]:

$$T_{11}(t = 0) = \frac{-8(1 + \beta)}{[(1 - \beta^2)Q^2 + \mu_q^2 - \mathbf{l}_t^2 + \mathbf{k}_t^2 - 2\mathbf{l}_t \cdot \mathbf{k}_t][(1 - \beta^2)Q^2 + \mu_q^2 - \mathbf{l}_t^2]}$$

$$\begin{aligned}
& \times \{ [\mathbf{l}_t^2 - (1 - \beta^2)Q^2 - \mu_q^2] (\epsilon_t \cdot \mathbf{l}_t e_t \cdot \mathbf{k}_t - \beta^2 \epsilon_t \cdot \mathbf{k}_t e_t \cdot \mathbf{l}_t - \mathbf{l}_t \cdot \mathbf{k}_t \epsilon_t \cdot e_t) \\
& + (1 - \beta^2) (\mathbf{k}_t^2 - 2\mathbf{l}_t \cdot \mathbf{k}_t) \epsilon_t \cdot \mathbf{l}_t e_t \cdot \mathbf{l}_t + (\mathbf{l}_t^2 - \mu_q^2)(2\mathbf{l}_t \cdot \mathbf{k}_t + \mathbf{k}_t^2) \epsilon_t \cdot e_t \}
\end{aligned} \tag{21}$$

2.2 The spin-flip amplitudes.

The calculation are similar than for the SCHC amplitudes. As the amplitudes conserve the parity at the vertex

$$\mathcal{A}_{-\lambda_V, -\lambda_\gamma} = (-1)^{\lambda_V - \lambda_\gamma} \mathcal{A}_{\lambda_V, \lambda_\gamma}$$

we have only three spin-flip amplitudes to calculate ($\mathcal{A}_{01}, \mathcal{A}_{10}, \mathcal{A}_{-11}$).

The two amplitudes \mathcal{A}_{01} et \mathcal{A}_{10} , derived from the Feynman diagrams (fig. 1), are given by:

$$T_{01}(\lambda_V = 0, \lambda_\gamma = +1) = \frac{N_{01}}{D}, \tag{22}$$

$$T_{10}(\lambda_V = +1, \lambda_\gamma = 0) = \frac{N_{10}}{D}, \tag{23}$$

with :

$$\begin{aligned}
D = & [2(1 - \beta) \mathbf{l}_t \cdot \Delta_t - \mathbf{l}_t^2 + \mu_q^2 + (1 - \beta^2)Q^2 - (1 - \beta)^2 t] \\
& \times [2(1 - \beta) \mathbf{l}_t \cdot \Delta_t + 2(1 - \beta) \mathbf{k}_t \cdot \Delta_t - 2\mathbf{l}_t \cdot \mathbf{k}_t \\
& + \mathbf{k}_t^2 - \mathbf{l}_t^2 + \mu_q^2 + (1 - \beta^2)Q^2 - (1 - \beta)^2 t],
\end{aligned} \tag{24}$$

$$\begin{aligned}
N_{01} = & \frac{4}{m_V} \beta (1 + \beta) [\mathbf{l}_t^2 - \mu_q^2 - (1 - \beta^2)m_V^2] \\
& \times \{ \epsilon_t \cdot \Delta_t (1 - \beta) [4(1 - \beta) \Delta_t \cdot \mathbf{k}_t + 2\mathbf{l}_t \cdot \mathbf{k}_t + \mathbf{k}_t^2] \\
& + 2\epsilon_t \cdot \mathbf{l}_t [\mathbf{l}_t \cdot \mathbf{k}_t - (1 - \beta) \Delta_t \cdot \mathbf{k}_t] \\
& + \epsilon_t \cdot \mathbf{k}_t [2(1 - \beta) \Delta_t \cdot \mathbf{l}_t - \mathbf{k}_t^2 - \mathbf{l}_t^2 + \mu_q^2 + (1 - \beta^2)Q^2 - (1 - \beta)^2 t] \},
\end{aligned} \tag{25}$$

$$N_{10} = -8 \beta \epsilon_L q (1 + \beta)^2 (1 - \beta) \mathbf{l}_t \cdot e_t [2\mathbf{k}_t \cdot \mathbf{l}_t - 2(1 - \beta) \mathbf{k}_t \cdot \Delta_t - \mathbf{k}_t^2]. \tag{26}$$

Performing the numerical calculations, we observe the following hierarchy:

$$|\mathcal{A}_{00}| > |\mathcal{A}_{11}| > |\mathcal{A}_{01}| > |\mathcal{A}_{10}| > \dots \tag{27}$$

for relatively high Q^2 . In the HERA kinematical range [5, 6], we find that the helicity amplitude $|\mathcal{A}_{10}|$, where a transverse meson is produced by a longitudinal photon, is of the order of 20 times smaller than the amplitude for the

production of a longitudinal meson by a transverse photon $|\mathcal{A}_{01}|$, itself 30 times smaller than the longitudinal amplitude \mathcal{A}_{00} . The double spin-flip amplitudes $A_{1-1} = A_{-11}$ are still smaller and are neglected in this work.

3 Amplitudes properties.

3.1 Case of a zero Fermi momentum: $l = 0 \rightarrow \beta = 0$.

The single spin-flip amplitudes \mathcal{A}_{01} (22) and \mathcal{A}_{10} (23) are proportional to the Sudakov coefficient β of the quark Fermi momentum ($l = \frac{t}{2} + \frac{\beta}{2}q + \frac{\alpha}{2w^2}p$). When $\beta = 0$ these ones become zero at the opposite of the two helicity conserving amplitudes \mathcal{A}_{00} (19) et \mathcal{A}_{11} (21). As we can see, the Fermi momentum plays an important role in the presence of \mathcal{A}_{01} and \mathcal{A}_{10} . The conditions $\beta = 0$ or $l_{\text{Fermi}} = 0$ imply s -channel helicity conservation.

3.2 Q^2 behaviour.

Figure 2 shows the Q^2 evolution of the different helicity amplitudes for a mean value of $|t|$ fixed ($|t| = 0.1352 \text{ GeV}^2$). We clearly see that the vector meson production amplitudes by a real longitudinal photon ($Q^2 = 0$), A_{00} and A_{10} , decrease to zero when $Q^2 \rightarrow 0$.

In photoproduction, as expected from the Ward identity, the expressions (19) and (26) are exactly zero:

$$\begin{aligned} T_{00} &= 0, \\ T_{10} &= 0, \end{aligned} \tag{28}$$

whereas $T_{11} \neq 0$ and $T_{01} \neq 0$.

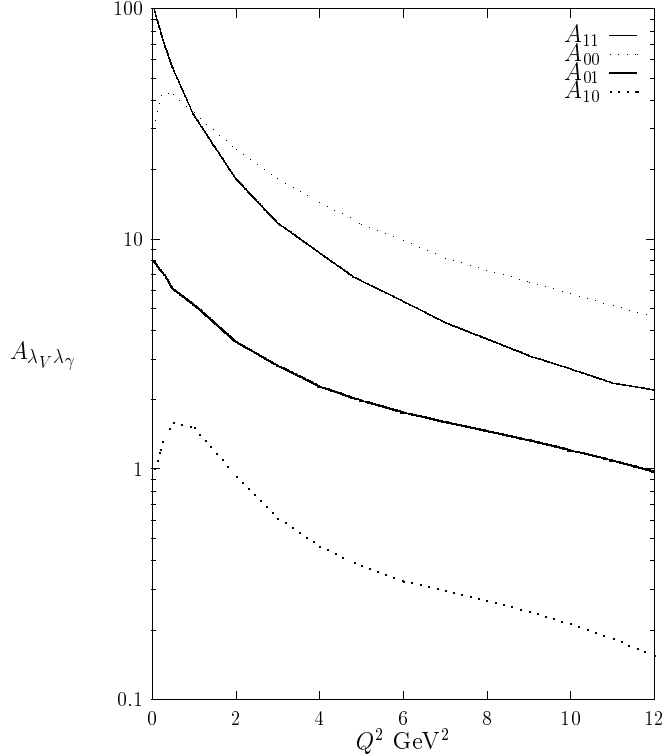


Figure 2: Q^2 dependence of the helicity amplitude for $\langle |t| \rangle = 0.1352$ GeV 2 .

For high- Q^2 , looking at the numerical results (fig. 2), we observe that the behaviour is more complex than expected by just taking the asymptotic limit of equations (19, 21, 22 and 23). The integration over l^2 and β introduces supplementary Q^2 terms in the contribution to T_{11} , T_{01} and T_{10} due to the off-shell quark. The Q^2 range at HERA is far from the asymptotic limit, as consequence, we are enable to control the asymptotic calculation of the amplitudes.

3.3 Low \mathbf{k}_t^2 behaviour.

As in the previous paper [2], the amplitudes are finite in the infrared region. Hence, (15) gives:

$$d\mathcal{A}_{\lambda_V \lambda_\gamma} \propto \frac{T_{\lambda_V \lambda_\gamma} \mathcal{F}(k, k - \Delta)}{\mathbf{k}_t^2 (\mathbf{k}_t - \Delta_t)^2}. \quad (29)$$

If we develop the $T_{\lambda_V \lambda_\gamma}$ expressions (eqs.19, 21, 22 and 23) in the region of small transverse gluon momentum $\mathbf{k}_t^2 \rightarrow 0$, we obtain:

$$d\mathcal{A}_{\lambda_V \lambda_\gamma}(\mathbf{k}_t^2 = 0) \propto \frac{\mathcal{F}(k, k - \Delta)}{(\mathbf{k}_t - \Delta_t)^2} \quad (30)$$

As the proton form factor can be expressed by $\mathcal{F}(k, k - \Delta) \propto \mathbf{k}_t \cdot (\mathbf{k}_t - \Delta)$ in the infrared region [13], all subsistent singularity of the denominator is canceled.

3.4 $|t| = 0$ behaviour.

As $|t| = |t_{min}| \approx 0$, we observe the cancellation of all the spin-flip amplitudes:

$$\mathcal{A}_{01} = \mathcal{A}_{0-1} = \mathcal{A}_{10} = \mathcal{A}_{-10} = \mathcal{A}_{1-1} = \mathcal{A}_{-11} = 0. \quad (31)$$

Figure 3 shows the $|t|$ dependence of all the helicity amplitudes for Q^2 fixed ($\langle Q^2 \rangle = 4.8 \text{ GeV}^2$). The single spin-flip amplitudes - A_{01} and A_{10} - cancel when $|t| = 0$, present a maximum at very small $|t| < 0.1 \text{ GeV}^2$ before decreasing for larger value of $|t|$.

Hence, in the high- Q^2 limit around $|t| = 0$, the ratio of T_{01} (where a longitudinal meson is produced by a transverse photon) and T_{00} (where a longitudinal meson is produced by a longitudinal photon), is the following:

$$\frac{T_{01}}{T_{00}} = \frac{\beta \sqrt{|t|}}{\sqrt{2}(1 + \beta) Q}. \quad (32)$$

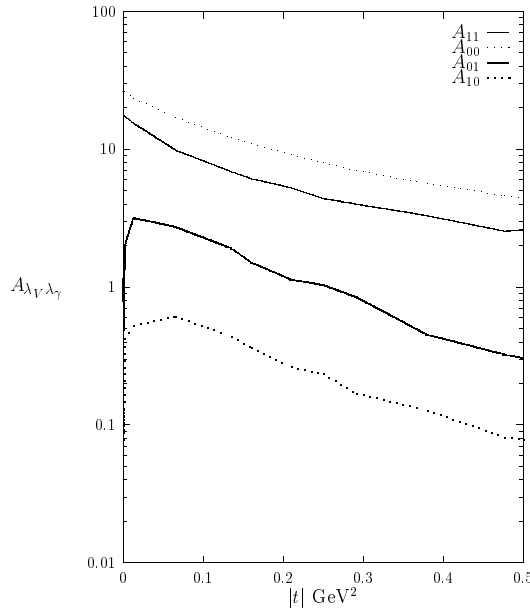


Figure 3: $|t|$ dependence of the helicity amplitudes for $\langle Q^2 \rangle = 4.8 \text{ GeV}^2$.

4 Matrix elements.

We have seen that spin-flip amplitudes are different from zero, in particular the amplitude A_{01} , where a longitudinal meson is produced by a transverse photon. Those amplitudes play a significant role in the behaviour of the 15 matrix elements measured by HERA.

Following [7] and the relations presented in the appendix A, we can derive the independent matrix elements r_{ik}^α .

Table 1 present the results obtained with our model (where $A_{-11} = A_{1-1}$ are neglected) for the different matrix elements in comparison with experimental data and the SCHC assumption in the case of ρ meson production.

Figures 4 and 5 illustrate respectively the Q^2 and $|t|$ dependence of the 15 spin density matrix elements in the case of ρ meson production. We can see that the model is in good agreement with the data from H1 [5] and ZEUS [6] even at low Q^2 . The presence of an SCHC violation is clearly observed for r_{00}^5 which is significantly different from zero. This element is indeed proportional to the most important spin-flip amplitude A_{01} .

We made also some prediction for the production of the vector meson ϕ . Figure 6 illustrates the Q^2 dependence of the 15 spin density matrix elements in the case of ϕ meson production.

5 Conclusion.

Although helicity conserving amplitudes A_{00}, A_{11} are dominant, we showed that we cannot neglect the spin-flip amplitudes. Among them, the single spin-flip amplitude A_{01} where a longitudinal meson is produced by a transverse photon is the most important. Its presence is the indication of an evident violation of the SCHC assumption in the case of ρ^0 meson production.

We also estimated the violation taking the ratio of the dominant spin-flip amplitude and the helicity conserving amplitudes:

$$r = \frac{|A_{01}|}{\sqrt{|A_{11}|^2 + |A_{00}|^2}} \approx r_{00}^5 \sqrt{\frac{1+R}{2R}} \approx 8.0 \pm 3.0\% \quad (\text{exp}) \quad (33)$$

$$\approx 14. \pm 0.8\% \quad (\text{model}) \quad (34)$$

calculated for $\langle Q^2 \rangle = 4.8 \text{ GeV}^2$ and $\langle |t| \rangle = 0.138 \text{ GeV}^2$.

The calculation of the different helicity amplitudes and the different spin density matrix elements allows us to compare our model with H1 and ZEUS observation, and to see, once again, a good agreement.

Acknowledgments

I thank J.R. Cudell for several useful discussions, and Barbara Clerbaux for providing me with her analyses of the data.

| Elements | | data | | | our model | SCHC et Parity |
|----------|--------------------------|--------|-------------|----------------------|-----------|---|
| 1 | r_{00}^{04} | 0.674 | ± 0.018 | -0.036 $+0.051$ | 0.76 | $\frac{\epsilon R}{1+\epsilon R}$ |
| 2 | $\text{Re } r_{10}^{04}$ | 0.011 | ± 0.012 | $+0.007$ -0.001 | 0.059 | 0 |
| 3 | r_{1-1}^{04} | -0.010 | ± 0.013 | $+0.004$ -0.003 | -0.001 | 0 |
| 4 | r_{00}^1 | -0.058 | ± 0.048 | $+0.013$ -0.011 | -0.018 | 0 |
| 5 | r_{11}^1 | 0.002 | ± 0.034 | $+0.006$ -0.006 | 0. | 0 |
| 6 | $\text{Re } r_{10}^1$ | -0.018 | ± 0.016 | $+0.010$ -0.014 | -0.033 | 0 |
| 7 | r_{1-1}^1 | 0.122 | ± 0.018 | $+0.004$ -0.005 | 0.119 | $\frac{1}{2} \frac{1}{1+\epsilon R}$ |
| 8 | $\text{Im } r_{10}^2$ | 0.023 | ± 0.016 | $+0.010$ -0.009 | 0.033 | 0 |
| 9 | $\text{Im } r_{1-1}^2$ | -0.119 | ± 0.018 | $+0.010$ -0.005 | -0.119 | $-r_{1-1}^1$ |
| 10 | r_{00}^5 | 0.093 | ± 0.024 | $+0.019$ -0.010 | 0.16 | 0 |
| 11 | r_{11}^5 | 0.008 | ± 0.017 | $+0.008$ -0.012 | 0.01 | 0 |
| 12 | $\text{Re } r_{10}^5$ | 0.146 | ± 0.008 | $+0.006$ -0.006 | 0.15 | $\frac{\sqrt{2}}{4} \frac{\sqrt{R}}{1+\epsilon R} \frac{\text{Re}(A_{11}A_{00}^\dagger)}{ A_{11} A_{00} }$ |
| 13 | r_{1-1}^5 | -0.004 | ± 0.009 | $+0.001$ -0.003 | -0.01 | 0 |
| 14 | $\text{Im } r_{10}^6$ | -0.140 | ± 0.008 | $+0.002$ -0.004 | -0.149 | $-\text{Re } r_{10}^5$ |
| 15 | $\text{Im } r_{1-1}^6$ | 0.002 | ± 0.009 | $+0.003$ -0.000 | 0.01 | 0 |

Table 1: The 15 density spin matrix elements for the elastic ρ meson production for $Q^2 = 4.8$ GeV 2 and $|t| = 0.138$ GeV 2 at H1 [5] in comparison with our predictions (where A_{-11} and A_{1-1} are neglected) and the SCHC assumption and parity conservation.

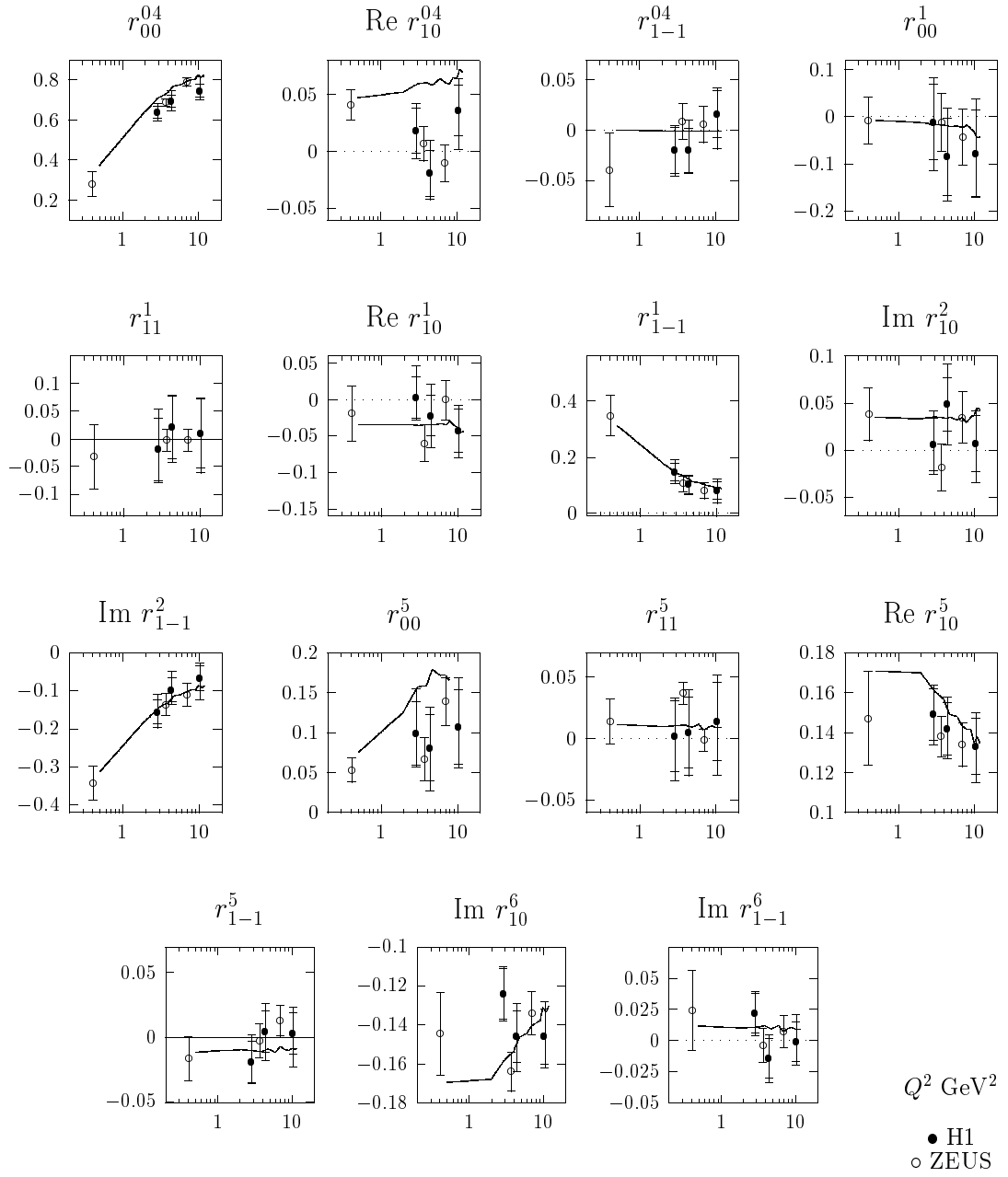


Figure 4: The Q^2 dependence of the 15 spin density matrix elements for the quasi-elastic ρ meson production compared to H1 [5] and ZEUS [6] data. The dashed line indicate the SCHC assumption. The solid lines are the predictions obtained with our model for $|t| = 0.138$ GeV 2 .

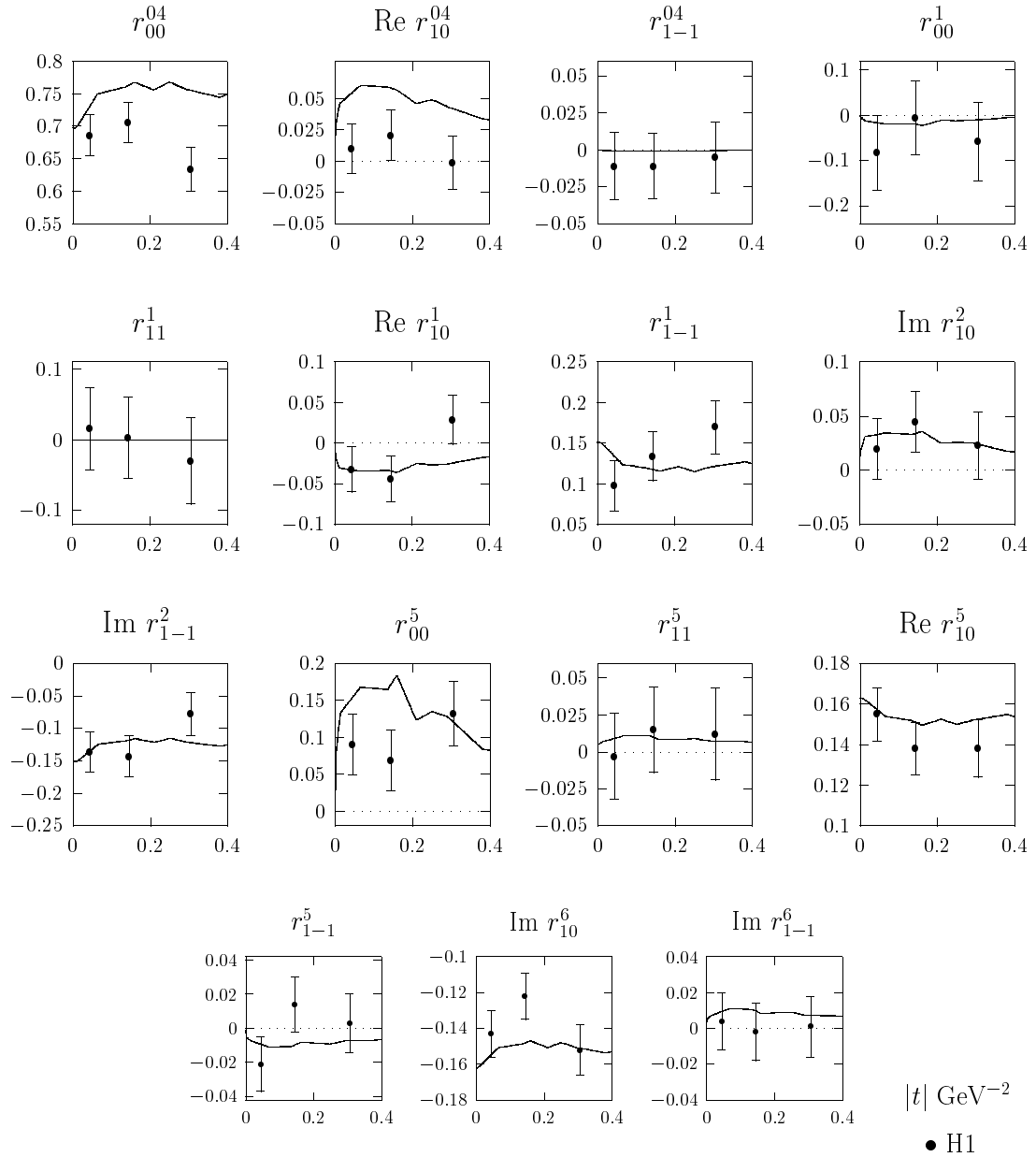


Figure 5: The $|t|$ dependence of the 15 spin density matrix elements for the *quasi-elastic* ρ meson production compared to H1 [5] data. The dashed line indicate the SCHC assumption. The solid lines are the predictions obtained with our model for $Q^2 = 4.8$ GeV 2 .

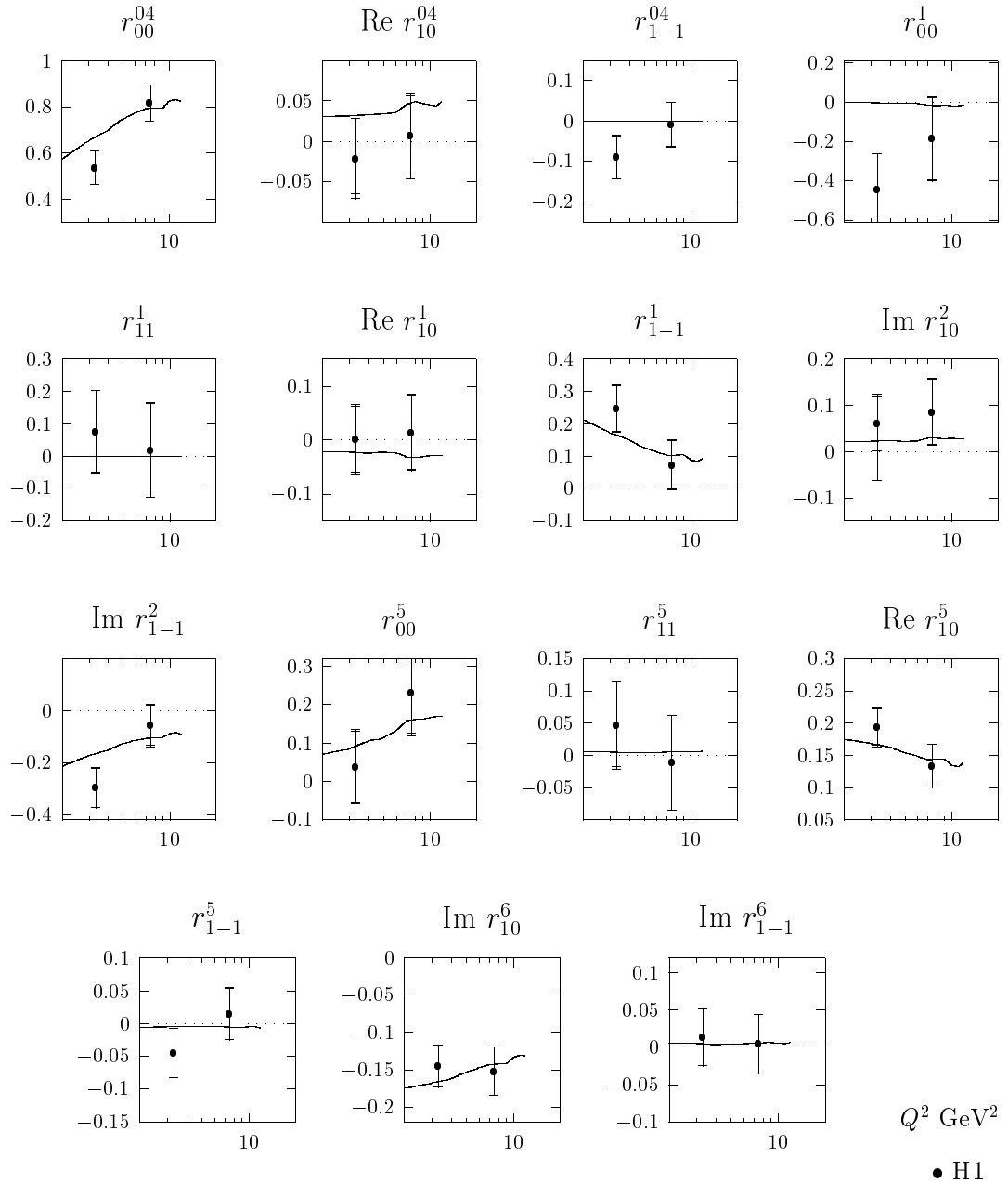


Figure 6: The Q^2 dependence of the 15 spin density matrix elements for the quasi-elastic ϕ meson production compared to H1 [14] data. The dashed line indicate the SCHC assumption. The solid lines are the predictions obtained with our model for $|t| = 0.138$ GeV 2 .

References

- [1] J.A. Crittenden, Springer Tracts in Modern Physics Volume 140 (Springer, Berlin, Heidelberg, 1997), hep-ex/9704009.
- [2] I. Royen, J. R. Cudell, *Nucl. Phys.* **B545** (1999) 505-525.
- [3] ZEUS Collaboration, J. Breitweg et al., *Eur. Phys. J.* **C6**(1999) 603; ZEUS Collaboration, M. Derrick et al., *Z. Phys.* **C69**(1995) 39; ZEUS Collaboration, J. Breitweg et al., *Eur. Phys. J.* **C2**(1998) 247; ZEUS Collaboration, M. Derrick et al., *Phys. Lett.* **B356** (1995) 601.
- [4] H1 Collaboration, S. Aid et al., *Nucl. Phys.* **B463** (1996) 3; H1 Collaboration, S. Aid et al., *Nucl. Phys.* **B468** (1996) 3; H1 Collaboration, C. Adloff et al., *Z. Phys.* **C75**(1997) 607.
- [5] H1 Collaboration, C. Adloff et al., *Eur. Phys. J.* **C13** (2000), 371.
- [6] ZEUS Collaboration, J.Breitweg et al., *Eur. Phys. J.* **C12** (2000), 393.
- [7] K. Schilling et G. Wolf, *Nucl. Phys.* **B61** (1973) 381.
- [8] D.Yu. Ivanov and R. Kirschner, *Phys. Rev.* **D58** (1998).
- [9] E.V. Kuraev, N.N. Nikolaev and B.G. Zakharov, *JETP Lett.* **68** (1998) 696.
- [10] S. J. Brodsky et G. P. Lepage, *Phys. Rev.* **D22** (1980) 2157.
- [11] M.G. Ryskin, R.G. Roberts, A.D. Martin et E.M. Levin, *Z. Phys.* **C76** (1997) 231, hep-ph/9511228.
- [12] M.G. Ryskin, *Sov. J. Nucl. Phys.* **52** (1990) 529, *Nucl. Phys. B (Proc. Suppl.)* **C18** (1991) 162.
- [13] J.R. Cudell and I. Royen, *Phys. Lett.* **397** (1997) 317.
- [14] H1 Collaboration, C. Adloff et al., DESY 00-070, May 2000, hep-ex/0005010, to be submitted to *Phys. Lett.* **B**.

A Relation between the 15 spin density matrix elements and the helicity amplitudes.

The expressions of the 15 spin density matrix elements given in this appendix are derived from the appendix A of [7].

The normalisation factors are defined as follow:

$$\begin{aligned} N_T &= \frac{1}{2} \sum_{\substack{\lambda_V, \lambda_{N'}, \\ \lambda_\gamma = \pm 1, \lambda_N}} |A_{\lambda_V \lambda_{N'}, \lambda_\gamma \lambda_N}|^2 \\ &= \frac{1}{2} [|A_{11}|^2 + |A_{-1-1}|^2 + |A_{01}|^2 + |A_{0-1}|^2 + |A_{-11}|^2 + |A_{1-1}|^2] \quad (35) \end{aligned}$$

$$\begin{aligned} N_L &= \sum_{\lambda_V, \lambda_{N'} \lambda_N} |A_{\lambda_V \lambda_{N'}, 0 \lambda_N}|^2 \\ &= |A_{00}|^2 + |A_{10}|^2 + |A_{-10}|^2 \end{aligned} \quad (36)$$

The matrix elements are combinations of helicity amplitudes:

$$r_{00}^{04} = \frac{1}{1 + \epsilon R} \left[\frac{1}{2N_T} (|A_{01}|^2 + |A_{0-1}|^2) + \frac{\epsilon R}{N_L} |A_{00}|^2 \right] \quad (37)$$

$$Re r_{10}^{04} = \frac{1}{1 + \epsilon R} Re \left[\frac{1}{2N_T} (A_{11} A_{01}^\dagger + A_{1-1} A_{0-1}^\dagger) + \frac{\epsilon R}{N_L} A_{10} A_{00}^\dagger \right] \quad (38)$$

$$r_{1-1}^{04} = \frac{1}{1 + \epsilon R} Re \left[\frac{1}{2N_T} (A_{11} A_{-11}^\dagger + A_{1-1} A_{-1-1}^\dagger) + \frac{\epsilon R}{N_L} A_{10} A_{-10}^\dagger \right] \quad (39)$$

$$r_{00}^1 = \frac{1}{1 + \epsilon R} \frac{1}{2N_T} (A_{0-1} A_{01}^\dagger + A_{01} A_{0-1}^\dagger) \quad (40)$$

$$r_{11}^1 = \frac{1}{1 + \epsilon R} \frac{1}{2N_T} (A_{1-1} A_{11}^\dagger + A_{11} A_{1-1}^\dagger) \quad (41)$$

$$Re r_{10}^1 = \frac{1}{1 + \epsilon R} \frac{1}{2N_T} Re (A_{1-1} A_{01}^\dagger + A_{11} A_{0-1}^\dagger) \quad (42)$$

$$r_{1-1}^1 = \frac{1}{1 + \epsilon R} \frac{1}{2N_T} (A_{1-1} A_{-11}^\dagger + A_{11} A_{-1-1}^\dagger) \quad (43)$$

$$Im r_{10}^2 = \frac{1}{1 + \epsilon R} \frac{1}{2N_T} Im [i(A_{1-1} A_{01}^\dagger - A_{11} A_{0-1}^\dagger)] \quad (44)$$

$$Im r_{1-1}^2 = \frac{1}{1 + \epsilon R} \frac{1}{2N_T} Im [i(A_{1-1} A_{-11}^\dagger - A_{11} A_{-1-1}^\dagger)] \quad (45)$$

$$r_{00}^5 = \frac{\sqrt{R}}{1 + \epsilon R} \frac{1}{\sqrt{2N_T N_L}} [Re(A_{00} A_{01}^\dagger - Re(A_{00} A_{0-1}^\dagger)] \quad (46)$$

$$r_{11}^5 = \frac{\sqrt{R}}{1 + \epsilon R} \frac{1}{\sqrt{2N_T N_L}} [Re(A_{10} A_{11}^\dagger - Re(A_{10} A_{1-1}^\dagger)] \quad (47)$$

$$Re r_{10}^5 = \frac{\sqrt{R}}{1+\epsilon R} \frac{1}{\sqrt{2N_T N_L}} \frac{1}{2} Re(A_{10}A_{01}^\dagger + A_{11}A_{00}^\dagger - A_{10}A_{0-1}^\dagger - A_{1-1}A_{00}^\dagger) \quad (48)$$

$$r_{1-1}^5 = \frac{\sqrt{R}}{1+\epsilon R} \frac{1}{\sqrt{2N_T N_L}} \frac{1}{2} (A_{10}A_{-11}^\dagger + A_{11}A_{-10}^\dagger - A_{10}A_{-1-1}^\dagger - A_{1-1}A_{-10}^\dagger) \quad (49)$$

$$Im r_{10}^6 = \frac{\sqrt{R}}{1+\epsilon R} \frac{1}{\sqrt{2N_T N_L}} \frac{1}{2} Re(A_{10}A_{01}^\dagger - A_{11}A_{00}^\dagger + A_{10}A_{0-1}^\dagger - A_{1-1}A_{00}^\dagger) \quad (50)$$

$$Im r_{1-1}^6 = \frac{\sqrt{R}}{1+\epsilon R} \frac{1}{\sqrt{2N_T N_L}} \frac{1}{2} Re(A_{10}A_{-11}^\dagger - A_{11}A_{-10}^\dagger + A_{10}A_{-1-1}^\dagger - A_{1-1}A_{-10}^\dagger) \quad (51)$$

where R is the ratio of the longitudinal and transverse cross sections γ^*p :

$$R = \frac{N_L}{N_T} = \frac{\sigma_L}{\sigma_T}. \quad (52)$$